### Title

Differential effects of Hsp90 inhibition on corneal cells in vitro and in vivo




### Authors

Raghunathan, VijayKrishna

Edwards, Sydney Garrison

Leonard, Brian C

et al.



### Publication Date

2021

### DOI

10.1016/j.exer.2020.108362

Peer reviewed

HHS Public Access

Author manuscript

*Exp Eye Res*. Author manuscript; available in PMC 2022 January 01.

Published in final edited form as:

*Exp Eye Res*. 2021 January ; 202: 108362. doi:10.1016/j.exer.2020.108362.

# Differential effects of Hsp90 inhibition on corneal cells *in vitro* and *in vivo*

**VijayKrishna Raghunathan**[1,2,*,#], **Sydney Garrison Edwards**[3,*], **Brian C Leonard**[3,*], **Soohyun Kim**[3], **Alexander T. Evashenk**[3], **Yeonju Song**[3], **Eva Rewinski**[3], **Ariana Marangakis Price**[3], **Alyssa Hoehn**[3], **Connor Chang**[3], **Christopher M Reilly**[3], **Santoshi Muppala**[3], **Christopher J Murphy**[3,4], **Sara M Thomasy**[3,4,#]

[1]Department of Basic Sciences, College of Optometry, University of Houston, Houston, TX

[2]The Ocular Surface Institute, College of Optometry, University of Houston, Houston, TX

[3]Department of Surgical and Radiological Sciences, School of Veterinary Medicine, University of California, Davis, Davis, CA

[4]Department of Ophthalmology and Vision Science, School of Medicine, University of California, Davis, Davis, CA

## Abstract

The transformation of quiescent keratocytes to activated fibroblasts and myofibroblasts (KFM transformation) largely depends on transforming growth factor beta (TGFβ) signaling. Initiation of the TGFβ signaling cascade results from binding of TGFβ to the labile type I TGFβ receptor (TGFβRI), which is stabilized by the 90 kDa heat shock protein (Hsp90). Since myofibroblast persistence within the corneal stroma can result in stromal haze and corneal fibrosis in patients undergoing keratorefractive therapy, modulation of TGFβ signaling through Hsp90 inhibition would represent a novel approach to prevent myofibroblast persistence.

*In vitro,* rabbit corneal fibroblasts (RCFs) or stratified immortalized human corneal epithelial cells (hTCEpi) were treated with a Hsp90 inhibitor (17AAG) in the presence/absence of TGFβ1. RCFs were cultured either on tissue culture plastic, anisotropically patterned substrates, and hydrogels of varying stiffness. Cellular responses to both cytoactive and variable substrates were assessed by morphologic changes to the cells, and alterations in expression patterns of key keratocyte and myofibroblast proteins using PCR, Western blotting and immunocytochemistry. Transepithelial electrical resistance (TEER) measurements were performed to establish epithelial barrier integrity. *In vivo,* the corneas of New Zealand White rabbits were wounded by phototherapeutic keratectomy (PTK) and treated with 17AAG (3x or 6x daily) either immediately or 7 days after wounding for 28 days. Rabbits underwent clinical ophthalmic examinations, SPOTS scoring and

[#]**Corresponding authors:** Sara M Thomasy, UC Davis School of Veterinary Medicine, Department of Surgical and Radiological Sciences, University of California, Davis, Davis, CA, 95616; smthomasy@ucdavis.edu; VijayKrishna Raghunathan, University of Houston College of Optometry, University of Houston, Houston, TX, 77204; vraghunathan@uh.edu.
[*]Authors contributed equally

advanced imaging on days 0, 1, 3, 7, 10, 14, 21 and 28. On day 28, rabbits were euthanized and histopathology/immunohistochemistry was performed.

*In vitro* data demonstrated that 17AAG inhibited KFM transformation with the de-differentiation of spindle shaped myofibroblasts to dendritic keratocyte-like cells accompanied by significant upregulation of corneal crystallins and suppression of myofibroblast markers regardless of TGFβ1 treatment. RCFs cultured on soft hydrogels or patterned substrates exhibited elevated expression of α-smooth muscle actin (αSMA) in the presence of 17AAG. Treatment of hTCEpi cells disrupted zonula occludens 1 (ZO-1) adherens junction formation. *In vivo*, there were no differences detected in nearly all clinical parameters assessed between treatment groups. However, rabbits treated with 17AAG developed greater stromal haze formation compared with controls, irrespective of frequency of administration. Lastly, there was increased αSMA positive myofibroblasts in the stroma of 17AAG treated animals when compared with controls.

Hsp90 inhibition promoted reversion of the myofibroblast to keratocyte phenotype, although this only occurred on rigid substrates. By contrast, *in vivo* Hsp90 inhibition was detrimental to corneal wound healing likely due to impairment in corneal epithelial closure and barrier function restoration. Collectively, our data demonstrated a strong interplay *in vitro* between biophysical cues and soluble signaling molecules in determining corneal stromal cell phenotype.

## 1. INTRODUCTION

Keratoablative surgical procedures such as laser-assisted in situ keratomileusis (LASIK) and photorefractive and phototherapeutic keratectomies (PRK and PTK) that require wounding of the central cornea are widely performed to correct refractive errors and treat anterior stromal disorders. Upon corneal stromal wounding, changes in the microenvironment of the wound promote transformation of the quiescent keratocyte to the activated fibroblast and subsequently the differentiated myofibroblast (KFM transformation). The involvement of the transforming growth factor (TGF) superfamily of cytokines in corneal wound repair is widely agreed upon, yet the two common isoforms TGFα and TGFβ have different roles in this process. TGFα is a component of the pre-corneal tear film (van Setten and Schultz, 1994) and aids in corneal epithelial cell migration, proliferation, and inhibits expression of differentiation marker Keratin 3 (Wilson et al., 1994). By contrast, TGFβ1 is secreted from corneal epithelial cells after wounding, which binds to TGF-β type I receptors (TGFβRI) and type II receptors (TGFβRII) in stromal cells, forming a stable complex that leads to receptor-dependent phosphorylation of Smad proteins and ultimate induction of αSMA expression, a potent marker for myofibroblast transdifferentiation (Hu et al., 2003; Zi et al., 2012).

We have documented biophysical attributes (stiffness and topography) to profoundly modulate fundamental corneal cell behaviors integral to corneal wound healing including adhesion, migration, proliferation, differentiation and response to growth factors (Fraser et al., 2008; Karuri et al., 2004; Karuri et al., 2006; Liliensiek et al., 2006; Pot et al., 2010; Tocce et al., 2010). Using a rabbit model for PTK and corneal wound healing, we recently demonstrated that *in vivo* stromal stiffening precedes KFM transformation during stromal wound repair (Raghunathan et al., 2017) and concomitantly demonstrated that stiffer

substrates promote TGFβ1-induced myofibroblast transformation of human and rabbit stromal fibroblasts *in vitro* (Dreier et al., 2013), supporting the critical role of mechanotransduction in cell-matrix interactions. These findings suggest that prolonged stiffening of the stromal microenvironment would increase the number and resident times of myofibroblasts whose retention leads to the formation of stromal haze, impairing corneal clarity and ultimately, patient vision. Currently, the standard of care is to treat patients with mitomycin C intraoperatively to limit post-surgical fibrosis. However, there is a subset of patients that go on to develop stromal haze despite this intervention. Thus, there is a need to identify therapeutics that can reduce corneal stromal haze without compromising the myofibroblast's function of remodeling the stroma, and minimizing persistence of the myofibroblasts in the wound space.

Prior reports demonstrate that the heat-shock protein 90 (Hsp90), a multifunctional molecular chaperone that facilitates protein folding (Pearl and Prodromou, 2006) and cytoskeleton stabilization by binding actin and tubulin (Czar et al., 1996), promotes the stability of glucocorticoid (Jayaprakash et al., 2015; Kirschke et al., 2014; Xu et al., 1998; Zhang et al., 2006) and TGFβ receptors (TβRs) (Wrighton et al., 2008) among other functions. Hsp90 consists of a highly conserved N-terminal domain (NTD), a middle domain (MTD), and a C-terminal domain (CTD). Activity of Hsp90 has traditionally been attributed to its ATP-dependent NTD(Pearl and Prodromou, 2006). A number of Hsp90 NTD inhibitors have been identified and several have entered clinical trials as anti-cancer drugs acting through the disruption of ATPase activity of Hsp90. The most widely studied NTD inhibitors are the geldanamycin analogs 17-Allylamino-17-demethoxygelanamycin (17AAG) and 17-Dimethylaminoethylamino-17-demethoxygeldanamycin (17DMAG). 17AAG inhibition of Hsp90 has been shown to target the TGF-β receptor complex for ubiquitination and proteasomal degradation to prevent fibrosis in non-ocular systems (Noh et al., 2012; Tomcik et al., 2014), but has gained limited attention in the cornea. Previously, we demonstrated that low concentrations of 17AAG, promoted the formation of cell-cell junctions and co-localization of E-cadherin and β-catenin at adherens junctions (Raghunathan et al., 2014) *in vitro*, suggesting that Hsp90 may be a druggable target for ameliorating development of recurrent corneal defects and promoting wound repair. However, its effects on corneal stromal cells or its ability to promote stromal wound repair remain unclear. Here we determine the effect of 17AAG on KFM transformation *in vitro* and *in vivo* using a rabbit phototherapeutic keratectomy model of corneal wound healing.

## 2. MATERIALS AND METHODS

### 2.1 In vitro studies

**2.1.1 Fabrication of substrates—**Polymeric substrates with biologically relevant size-scale anisotropic topography (Planar (control), 1400nm pitch; pitch = groove + ridge width) and hydrogels of different elastic moduli (5, 25 kPa) were fabricated as described previously (Dreier et al., 2013; Thomasy et al., 2018; Wood et al., 2011). The choice of 1400 nm pitch anisotropically patterned topography was based on our previous reports (Myrna et al., 2012; Pot et al., 2010) wherein we demonstrated that this size scale topography suppressed development of the myofibroblast phenotype even in the presence of TGFβ. The choice of

elastic moduli of the hydrogels were based on prior studies that identified representative moduli of corneal stroma under normal (soft) and wounded (stiff) conditions (Dreier et al., 2013; Thomasy et al., 2014).

**2.1.2 Stromal cell culture—**Primary rabbit corneal stromal cells were isolated as previously described (Dreier et al., 2013) from freshly enucleated young rabbit eyes (Pel-Freeze, Rogers, AR). Cells were cultured on tissue culture plastic, planar or anisotropically patterned substrates, and hydrogels, in DMEM low glucose supplemented with 10% fetal bovine serum (FBS) and 1% penicillin/streptomycin/fungizone (P/S/F), in the presence or absence of 10 ng/ml TGFβ1, and/or 500 nM 17AAG. The dose of 17AAG required was determined empirically by a dose-response curve where toxicity or gross alterations to cellular morphologically was assessed by microscopic evaluation using phase contrast, MTT viability assay (Sigma-Aldrich, St. Louis, MO), and calcein-AM/ethidium homodimer labelling (ThermoFisher, CA). As a positive control for cell death, staurosporine was used. Experiments were performed in triplicate.

**2.1.3 Epithelial cell culture—**Immortalized human corneal epithelial cells (hTCEpi) (Robertson et al., 2005), kindly provided by Dr James V Jester (UC Irvine), were maintained in EpiLife medium supplemented with EpiLife defined growth supplement (EDGS; Life Technologies), 1% P/S/F (Life Technologies) and were used between passages 40-60. Cells were cultured at 37°C and 5% $CO_2$ until they reached 100% confluence, and the basal growth media (GM) was replaced by stratification media (SM) containing DME/F12 medium (Invitrogen), 10% FBS, 10 ng/mL EGF, 1% P/S/F to induce differentiation and stratification (Argüeso and Gipson, 2012). Stratification was optimized and verified as described previously (Yanez-Soto et al., 2015). hTCEpi cells were then incubated with DMSO control or 17AAG at varying concentrations to determine a non-toxic dose (Mosmann, 1983). Subsequently, cells were cultured in Costar® 12mm Snapwell™ transwell inserts 0.4μm pore size, polycarbonate membrane) for measuring transepithelial electrical resistance (TEER) or cultured on glass coverslips for immunocytochemistry. Cells were treated with 5 or 10 μM 17AAG for 24 h.

**2.1.4 Transepithelial electrical resistance (TEER) measurements—**Electrical resistance of stratified epithelial cells in the presence or absence of 17AAG was measured using the Millicell ERS voltohmmeter (Millipore-Sigma) following manufacturer guidelines. Blank resistance was measured using a cell culture insert without cells. Five measurements per sample were recorded with at least three samples per experiment. Resistance values were normalized to blank controls and multiplied by the effective membrane area to arrive at the final resistance of a unit area. Experiments were performed in triplicate.

**2.1.5 Quantitative real time polymerase chain reaction (qRT-PCR)—**Total RNA was isolated using an RNA purification kit (GeneJET Plasmid Miniprep Kit; ThermoFisher Scientific, CA) following the manufacturer's instructions and equal amounts (60 ng) were used for the qPCR reactions. qPCR was performed using a reagent kit (SensiFAST™ Hi-ROX One-Step Kit; Bioline USA Inc, Taunton, MA) and commercially available and validated aptamers for *GAPDH* (Oc03823402); *KERA* (Oc03396149); and *ACTA2*

(Oc03399251); *COL3A1* (Oc04096544); *ALDH1A1* (Oc03396767_m1) in total volumes of 10 μL per reaction (ThermoFisher Scientific, CA). The reverse transcription reaction was performed (StepOne; ThermoFisher Scientific, CA) with the following parameters: 30 minutes at 50°C followed by 10 minutes at 95°C; 40 cycles of 60°C for 1 minute followed by 95°C for 15 seconds. Relative expression of mRNAs of interest were determined as described previously (Raghunathan et al., 2013).

**2.1.6 Immunocytochemistry—**Immunocytochemistry was performed as described previously (Dreier et al., 2013). Briefly, cells were fixed in 4% paraformaldehyde for 20 min, further permeabilized with 0.01% Triton X-100 in phosphate buffered saline (PBS, pH 7.4), blocked with 3% fish gelatin, immunolabelled with anti-α-smooth muscle actin (αSMA; Sigma-Aldrich) and species appropriate fluorescent conjugated secondary antibody (FisherScientific, CA), F-Actin was labelled with Phalloidin-594 (Life Technologies), and nuclei were counterstained with DAPI (FisherScientific, CA). For each immunostained sample, 5-10 random locations were imaged using a Zeiss Axiovert 200M (Carl Zeiss, Germany) inverted fluorescence microscope. Due to the qualitative nature of imaging, no quantitative measurements were performed at this time. As appropriate, representative images from a single field of view for a single donor are illustrated in the results section(s).

**2.1.7 Western Blotting—**RCF cells treated with/without 17AAG were lysed into RIPA buffer, denatured using NuPAGE LDS sample buffer and run on denaturing 4-12% gradient polyacrylamide gels (NuPAGE Bis-Tris gels, Life technologies, Grand Island, NY, USA) and transferred onto nitrocellulose membranes. Blots were blocked using SuperBlock (ThermFisher) for 1h, and incubated with anti-Hsp90 (Cell Signaling Technologies) or β-actin (Abcam) overnight at 4°C on a rotating shaker. The membranes were washed thrice with phosphate buffered saline with Tween-20 and incubated with corresponding HRP-conjugated secondary antibody for 90 minutes at room temperature. The proteins were then visualized using ECL detection reagents (SuperSignal West Femto Maximum Sensitivity Substrate; Life technologies, Grand Island, NY, USA) on a ChemiDoc-It2 810 Imaging system (UVP, CA).

## 2.2 In vivo studies

The *in vivo* studies were approved by the Institutional Animal Care and Use Committees of the University of California-Davis (Protocols #17289, #20022) and were performed according to the Association for Research in Vision and Ophthalmology resolution on the use of animals in research.

**2.2.1 Animals—**Eighteen New Zealand White rabbits with a mean ± SD age of 3.4 ± 0.8 months and weight of 3.7 ± 0.8 kg were included.

**2.2.2 Epithelial debridement and phototherapeutic keratectomy (PTK)—**Rabbits were sedated with 0.7 mg/kg midazolam and 0.1 mg/kg hydromorphone intramuscularly for examinations, and as pre-medication; plus an additional administration of 15-25 mg/kg ketamine IM to induce anesthesia prior to surgery. Inhalational isoflurane was used only when needed for additional anesthesia during PTK. On the day of wounding

(Day0; D0), the central corneal epithelium was debrided (8 mm diameter) OD with an excimer spatula (Visitec® Excimer Spatula, Lindstrom/Vorkas, Miami, FL, USA). Fluorescein stain (Bausch & Lomb, Rochester, NY, USA) was used to confirm that all the epithelium was removed. All rabbits then received a 6 mm diameter, 100 μm depth PTK (corneal surgery excimer laser; EC-5000, Nidek, Freemont, CA, USA) on the right eye (oculus dexter, OD). The left eye (oculus sinister, OS) remained unwounded to serve as a control. Following surgery, all rabbits received buprenorphine 0.045 mg/kg subcutaneously (SC) every 12 h (Buprenex 0.3 mg/mL injection solution, Reckitt Benckiser Group pic, Slough, Berkshire,UK), and a drop of ofloxacin 0.3% ophthalmic solution OD every 12 h until the cornea no longer retained fluorescein stain.

**2.2.3 17AAG application—**Rabbits were randomly assigned to 1 of 3 experimental groups, and immediately after undergoing PTK, rabbits (6 rabbits per experimental group) were treated topically in both eyes either with **A.** vehicle control only three times daily (25% DMSO), **B.** 100 μM 17AAG three times daily or **C.** 100 μM 17AAG six times daily. The concentration of 17AAG used for *in vivo* experiments was chosen based on a prior dose escalation study that determined 100 μM to be the highest tolerated dose without adverse events observed using the SPOTs scoring system (Eaton et al., 2017). Power analysis ($p=0.05$, power=0.973, t-test) indicated 6 animals would be necessary when differences of the means between groups are moderate (0.5) and the standard deviations are large (0.2).

### 2.2.4 Clinical Characterization of Wounds

**2.2.4.1 Baseline Examinations:** Prior to surgery, baseline examinations were performed on all rabbits which consisted of pre- and post-dilated examination using slit lamp biomicroscopy [SL-15 portable slit lamp (Kowa American Corporation, Torrance, CA, USA) and indirect ophthalmoscopy (Pan Retinal 2.2 Biolens; Volk Optical, Inc. Mentor, OH, USA). Advanced diagnostics and imaging included: ultrasonic pachymetry (USP; AccuPach VI pachymeter, Accutome, Inc, Malvern, PA, USA) and Fourier-domain optical coherence tomography (FD-OCT; RTVue 100.Version 6.1 Optovue Inc. Fremont, CA, USA). Animals were scored using the SPOTS scoring system (Eaton et al., 2017) and a previously described semiquantitative scoring system for stromal haze (Raghunathan et al., 2017). External photographs were obtained with a digital single lens reflex (DSLR) camera (Canon ROS 5D, Canon Inc., Tokyo, Japan) at an aperture of *f*/18 or *f*/22 (Canon Macro Lens EF 100 mm 1:2:8) and flash setting at ¼ (Canon Macro Twin Lite MT-24EX 58 mm), while fluorescein images were taken with a previously described system (Kim et al., 2020).

**2.2.4.2 Ophthalmic examination, imaging and scoring:** Immediately after surgery on D0, and once daily thereafter for 7 days as well as on days 10, 14, 21, and 28 both eyes were examined using slit lamp biomicroscopy, scored using the SPOTs system, central corneal thickness measured with ultrasound pachymetry, external color and fluorescein photography performed, and FD-OCT corneal images obtained (Eaton et al., 2017). Corneal measurements (total, epithelial and stromal central corneal thickness, depth/thickness, and width of stromal haze in the axial cornea) were generated manually by one operator from each scan, using the caliper function integrated into the OCT software. If by D7, complete

re-epithelialization had not occurred, slit lamp biomicroscopy and fluorescein stain/photography were performed daily until complete re-epithelialization was noted.

**2.2.4.3 Wound Healing:** All fluorescein images were analyzed using a Java-based image processing system (Image J, National Institutes of Health, Bethesda, MD, USA), to calculate percentage wound closure as previously described (Park et al., 2015). Briefly, the outer and inner borders of the wound were traced and the area inside the borders was calculated. The area between these edges was the inwardly advancing newly epithelialized cornea. Percentage wound closure at each time point was calculated as:

$$\%\ Wound\ closure = \frac{Wound\ area\ on\ day\ 0 - Area\ of\ inner\ circumference\ on\ day\ X}{Wound\ area\ on\ day\ 0} x\ 100$$

**2.2.4.4 Euthanasia and Harvesting:** After examination on day 28, all rabbits were euthanized using pentobarbital (200 mg/kg, IV). The corneoscleral rim OD and OS were removed and processed for immunohistochemistry.

**2.2.5 Immunohistochemistry—**Immediately following euthanasia, the corneoscleral rim from both eyes were removed using corneal section scissors, rinsed with balanced salt solution, and placed in 10% neutral buffered formalin for at least 24 hours. These tissues were routinely processed, embedded in paraffin wax, and sections cut at 4 microns. Sections were then stained with hematoxylin and eosin or with primary antibodies. For immunohistochemistry, paraffin from the embedded sections was dissolved with xylene and tissue sections were serially dehydrated in ethanol. Antigen retrieval was performed in pH 6.0 citrate buffer at 95°C for 20 min. Sections were then blocked in ice cold 0.03 % (v/v) $H_2O_2$ in methanol. Immunohistochemical staining was performed for antibodies to α-SMA (mouse monoclonal, 1:100 dilution; Sigma-Aldrich), IgG (mouse monoclonal, Dako, 1:100 dilution), or α-tubulin (mouse monoclonal, Dako, 1:100 dilution). Species appropriate fluorophore conjugated secondary antibody labeling was performed (ThermoScientific, Rockford, IL). Sections were counter stained with DAPI and mounted in MOWIOL with 2.5% (w/v) DABCO as anti-fade. Images were acquired using an Olympus FluoView FV1000 confocal microscope (Olympus, CA).

## 2.3 Statistical analysis

**2.3.1 In vitro:** For all *in vitro* experiments on tissue culture plastic, two-way ANOVA was used to compare experimental groups with interactions between TGFβ and 17AAG treatment. For all *in vitro* experiments conducted on topographically patterned/variably compliant hydrogels, three-way ANOVA was used to compare experimental groups with interactions between substratum, TGFβ and 17AAG treatment using GraphPad Prism 8. Data are represented as bar plots (mean ± standard error of the mean) with experimental means (n=3) illustrated as individual points.

**2.3.2 In vivo:** Results from clinical evaluations and advanced imaging were analyzed using descriptive univariate analysis where the mean and standard deviation are reported. For epithelial and stromal wounding data, median scores for each time point were compared

using a non-parametric two-way analysis of variance on ranks (two-way ANOVA; Kruskal Wallis). Data are represented as median ± upper/lower limits.

## 3. RESULTS

### 3.1 Inhibition of Hsp90 changes stromal cell morphology in vitro

The RCFs were treated with vehicle control (DMSO) or 17AAG at varying concentrations (100 nM to 1 μM) for 24 h after which cell viability was assessed using the MTT assay. Significant loss of cell viability/proliferation was observed at a concentration greater than equal to 750 nM (Supplementary Fig S1A). The maximum dose at which we did not observe loss of cell proliferation was 500 nM and thus used in subsequent experiments. Prior to this, the ability of 500 nM 17AAG to reduce Hsp90 expression was documented by Western blotting. Indeed, Hsp90 protein expression was significantly lower than control group (Supplementary Fig S1B). 17AAG treated cells, both in the presence or absence of TGFβ1 exhibited a stellate morphology, typical of keratocytes (Figure 1A). Since Hsp90 is ubiquitously expressed in many cell types and regulates multiple metabolic pathways, we next determined if cell viability was affected by 17AAG using calcein-AM labelling. No significant differences were observed between ±TGFβ and ±17AAG interactions, although staurosporine treatment, the positive control for loss of viability, demonstrated significantly decreased calcein-AM signal labeling (Figure 1B).

### 3.2 Inhibition of Hsp90 reduced myofibroblast markers while upregulating keratocyte markers

In the absence of 17AAG, TGFβ1 treatment resulted in downregulation of keratocyte markers (*KERA* and *ALDH1A1*) while a marker for myofibroblast (*ACTA2*, the gene that encodes αSMA) was significantly elevated (3-fold, $p<0.05$) (Figure 2A). No differences were observed in Collagen Type III Alpha 1 Chain (*COL3A1*; a marker for myofibroblast activation,) expression with TGFβ1 treatment. In the presence of 17AAG, regardless of TGFβ1 treatment, significant upregulation of *KERA* and *ALDH1A1* was observed (*KERA:* > 3-fold, $p<0.05$; *ALDH1A1:* >5-fold, $p<0.001$) while mRNA expressions of *COL3A1* (<0.5-fold, $p<0.001$) was significantly inhibited. *ACTA2* expressions was dramatically abrogated in the absence or presence of TGFβ1 (<0.3-fold, $p<0.001$ or <0.7-fold, $p<0.01$ respectively) in RCFs co-treated with 17AAG. Expression of αSMA was validated by immunocytochemistry, which demonstrated significant inhibition of its immunostaining in RCFs stimulated with TGFβ1 and co-treated with 17AAG (Figure 2B).

### 3.3 Inhibition of Hsp90 immediately after wounding differentially affects wound healing in rabbits

Having confirmed the *in vitro* potency of 17AAG to promote retention of a keratocyte phenotype in the presence of TGFβ we set out to determine if this *in vitro* finding translated *in vivo* to corneal wound repair. Using a previously validated rabbit PTK corneal wounding model (Raghunathan et al., 2017), we evaluated the efficacy of 17AAG treatment to reduce corneal stromal haze formation in the context of corneal wound healing. Specifically, we evaluated the effect of 17AAG delivered topically either thrice daily or six-times daily

compared with placebo control, over several days, with treatment starting immediately after wounding.

Total conjunctivitis scores, obtained from the summation of conjunctival hyperemia and chemosis scores, were increased 1-5 days post PTK, and returned to near baseline by day 10; however, there were no differences (p=0.99) detectable between groups (Figure 3A). Total uveitis scores obtained from the summation of aqueous flare, cell and iris hyperemia scores over time was most evident on day 0 (day of the PTK) and returned rapidly back to baseline by day 2 post-PTK. No significant differences (p=0.93) in uveitis score were observed between groups (Figure 3B).

All epithelial wounds were healed by day 10, and wound healing rate did not significantly differ between groups (Figure 3C, p=0.89). However, it should be noted that on day 14, one rabbit from each of the 3x and 6x a day 17AAG treatment groups re-developed epithelial defects. On day 21, one placebo rabbit and two additional rabbits from each of the 3x/day and 6x/day 17AAG groups re-formed epithelial defects, making a total of 3 rabbits, or 50% of the rabbits in each 17AAG treatment group with recurrence of epithelial defects (Figure 3D). On day 28 the placebo rabbit healed, and epithelial defects persisted in only one each from 3x and 6x a day 17AAG groups. No significant changes in intraocular pressure were observed between the groups (Supplementary Figure S2).

Using slit lamp biomicroscopy we observed the development of stromal haze (Figure 4A) beginning around day 5 that steadily increased until the last day of the study, day 28. Contrary to our hypothesis, the 6x/day 17AAG treatment group had greater haze than the vehicle control group, with rabbits in the 6x/day 17AAG treatment group having a median stromal haze score of 1.2 (Figure 4B,C), and in the vehicle control group having a median stromal haze score of 0.89. Rabbits is the 3x/day 17AAG treatment group had a median stromal haze score of 1.06, which was not different to the other groups.

Stromal haze measured by FD-OCT using the caliper tool to determine stromal haze thickness, was in agreement with slit lamp biomicroscopy findings (Figure 4D). Advanced imaging of stromal haze using FD-OCT was apparent by day 5 and continued to increase until day 28 of the study. Unexpectedly, the 6x/day 17AAG treatment group, had greater (p=0.033) haze thickness measured from the anterior to posterior stroma (median: 80 ± 12 μM) than the vehicle control group (median: 57 ± 10 μM; Figure 4E,F). Rabbits in the 3x/day 17AAG treatment group had an intermediate haze thickness (median: 72 ± 14 μM), which was not significantly different from the other groups. Next, using immunohistochemistry we documented if αSMA expression corroborated our stromal haze scoring and thickness measurements. Indeed, increased immunostaining for αSMA was observed in 6x/day and 3x/day 17AAG compared with control groups (Figure 5).

### 3.4 *Substratum properties differentially modulate Hsp90 inhibition responses* in vitro

Since our *in vivo* data was contrary to *in vitro* data and our initial hypothesis; that rather than inhibiting development of myofibroblasts, 17AAG treatment resulted in increased myofibroblasts and stromal haze accompanied by corneal epithelial defects, we were curious

if the effect of Hsp90 inhibition in RCFs was dependent (at least partially) on substratum biophysical attributes.

To this end, informed by our previous studies, we cultured RCFs on either biologically relevant topography (Myrna et al., 2012; Pot et al., 2010) or hydrogels of relevant stiffness (Dreier et al., 2013). The 5-fold difference between 5 kPa and 25 kPa hydrogels represent the difference between a normal and wounded corneal stroma in rabbits. Using qPCR we documented changes in one keratocyte *(KERA)* and one myofibroblast *(ACTA2)* marker. We determined that on 1400 nm anisotropically patterned substrates, 17AAG, regardless of TGFβ1, overexpressed *KERA* expression significantly more than on planar surfaces (Figure 6A). While on planar substrates 17AAG inhibited *ACTA2* expression, on 1400 nm pitch anisotropically patterned substrates its expression was >3-to-4 fold elevated with 17AAG treatment compared with either vehicle control group or that on planar substrates. Concurrently, on these topographically patterned substrates, αSMA immunostaining was elevated with simultaneous treatment of 17AAG and TGFβ1 (Figure 6B). Finally, on 5 kPa polyacrylamide hydrogels, 17AAG treatment had no significant effect on *KERA* expression irrespective of TGFβ1 treatment (Figure 7). However, on the same gels, 17AAG treatment resulted in significant overexpression of *ACTA2*. On 25 kPa polyacrylamide hydrogels, 17AAG treatment resulted in significant upregulation on *KERA* expression irrespective of TGFβ1 treatment. Though, on the same gels, in the presence of TGFβ1, 17AAG treatment resulted in significant inhibition of *ACTA2* mRNA. Together these data suggest RCFs would become stimulated towards a myofibroblast phenotype on soft substrates; therefore, we speculated that treatment with an Hsp90 inhibitor when the stroma exhibited the highest stiffness post-wounding would lead to reduced persistence of myofibroblasts and *ACTA2* expression.

### 3.5 Delayed initiation of treatment with an Hsp90 inhibitor at peak corneal stiffness does diminish corneal stromal haze formation

In order to test our hypothesis that inhibition of Hsp90 initiated at a point when the stroma is stiffer would be more effective in haze reduction, we began 17AAG treatments on wounded eyes from the day the cornea was stiffest i.e day 7 after wounding (Raghunathan et al., 2017). Contrary to our expectations, we observed that Hsp90 inhibition from day 7 onwards did not decrease stromal haze formation during wound repair. We found no statistical differences in conjunctival/uveal scores, percentage epithelial wound healing, stromal haze score/thickness, between control and 17AAG groups (Supplementary Figure S3). However, recurrence of epithelial defects occurred suggesting the muted efficiency of Hsp90 inhibition may partially be due to lack of epithelial wound closure.

### 3.6 Inhibition of Hsp90 disrupts epithelial barrier function

Since stromal wounding was unaffected but reformation of epithelial defects occurred regardless of when 17AAG treatment began, we determined whether epithelial barrier function was compromised. For this, first, we incubated stratified hTCEpi cells, in a transwell insert, with DMSO vehicle control, 5μM or 10 μM 17AAG. By measuring TEER, we demonstrated significant loss of resistance with 17AAG treatment (Figure 8). This was accompanied by a significant reduction in immunostaining for ZO-1 which localizes to tight

junctions (Supplementary Figure S4). Collectively, these data demonstrate that continuity in the epithelial barrier was lost with 17AAG treatment.

## 4. DISCUSSION

Hsp90 is an abundant molecular chaperone that functions by stabilizing proteins to regulate a number of processes such as cell growth, survival, and differentiation (Pratt and Toft, 2003). Chaperone activity of Hsp90 is largely regulated by its ATPase-dependent activation (Grenert et al., 1999). Geldanamycin has been demonstrated to bind to the N-terminal ATP/ADP-binding domain of Hsp90 thus limiting its ATPase activity and subsequent function as a molecular chaperone (Grenert et al., 1997; Roe et al., 1999). Wrighton et al (Wrighton et al., 2008) identified TGFβRI and TGFβRII as Hsp90-interacting proteins and demonstrated that Hsp90 inhibition with 17AAG increased ubiquitination and degradation of TGFβ receptors thus blocking the TGFβ signaling pathway. Since the TGFβ pathway is critically implicated in corneal wound healing response and KFM transformation (Fini, 1999; Folger et al., 2001; Funderburgh et al., 2001; Jester et al., 1999; Kaur et al., 2009; Sakamoto et al., 2000; Tandon et al., 2010), we evaluated the effect of disrupting the TGF signaling pathway via Hsp90 inhibition in rabbit stromal cells *in vitro* and *in vivo*.

*In vitro* we verified that treatment of RCFs with 17AAG suppressed expression of downstream targets of TGFβ pathway and markers of corneal myofibroblasts, in the presence or absence of TGFβ1. This was accompanied by an increase in expression of biomarkers of corneal keratocytes, regardless of TGFβ1 treatment or presence of serum in the growth media. Congruent with these changes, the cultured stromal cells assumed the stellate/dendritic morphology characteristic of keratocytes. The occurrence of repair fibroblast phenotype and myofibroblast transformation in the presence of serum or TGFβ1 is associated with increased degradation of corneal crystallins (Stramer et al., 2001; Stramer and Fini, 2004) as observed here in the absence of Hsp90 inhibition. On the other hand, enhanced expression of these corneal crystallins is shown to decrease cellular light scattering(Jester et al., 2012) essential for the maintenance of corneal transparency. In aggregate, the data obtained from these *in vitro* investigations strongly pointed to 17AAG inhibiting myofibroblast generation and promoting retention of the homeostatic keratocyte phenotype. These findings motivated pursuing *in vivo* investigations to test the hypothesis that treatment with 17AAG would result in improving wound healing outcomes in rabbits undergoing PTK.

Immediately after creating of corneal wounds with PTK, we treated corneal tissues with vehicle control (DMSO) or 17AAG either three or six times daily over 28 days. Between our control and 17AAG treated groups, we did not observe any difference in IOP measurements, or incidence of conjunctivitis/uveitis, and percentage of epithelial wound closure. Although our control treatment was comprised of 25% (v/v) DMSO, our results demonstrated that it did not adversely affect the rate of wound healing. Further, in apparent contrast to our *in vitro* observations, we observed 17AAG treatment to result in a significant increase in epithelial re-ulceration that was accompanied with stromal haze and persistence of αSMA positive stromal cells (myofibroblasts). Formation of haze and myofibroblast occurrence in control groups during stromal remodeling at later time points (e.g days 21/28) were

consistent with earlier findings by us and others (de Medeiros et al., 2008; Netto et al., 2006; Raghunathan et al., 2017; Torricelli et al., 2016; Wilson, 2002). Of importance, our rationale for treatment of 17AAG immediately after wounding was due to the relationship between stromal stiffening and myofibroblast occurrence. In a previous study (Raghunathan et al., 2017), we showed that while corneal stromal stiffness was greatest 7 days after wounding, the maximal number of myofibroblasts was documented on day 21 post PTK in rabbits. Thus, we anticipated that 17AAG treatment preceding stromal stiffening would be beneficial. This however was not the case in our first set of *in vivo* experiments.

Next, we determined if 17AAG modulated stromal cell fate as function of substratum properties. Prior research from our group and others established that both topography and stiffness influence stromal cell phenotypes and KFM transformation (Dreier et al., 2013; Grinnell and Petroll, 2010; Karamichos et al., 2007; Kivanany et al., 2018; Lakshman and Petroll, 2012; Myrna et al., 2012; Petroll et al., 2015; Petroll and Lakshman, 2015; Petroll and Miron-Mendoza, 2015; Pot et al., 2010). Of key importance was our previous finding that anisotropically patterned surfaces (1400 nm pitch) facilitated the suppression of myofibroblast formation in the presence of TGFβ1(Myrna et al., 2012; Pot et al., 2010) and was thus our choice of patterned substrate in this study. As expected, in the absence of 17AAG, expression of *ACTA2*/αSMA was suppressed on topographically patterned surfaces in the presence or absence of TGFβ1. Interestingly, in the presence of 17AAG, while on planar surfaces *ACTA2*/αSMA expression was suppressed and *KERA* expression was elevated, however, on topographically patterned surfaces, both *ACTA2* and *KERA* expression was upregulated. This is likely due to a complex interaction between cytoskeletal remodeling and substratum topography (Andersson et al., 2003; Au et al., 2007; Dreier et al., 2012; Fraser et al., 2008; Petroll et al., 2015; Tabdanov et al., 2018; Teixeira et al., 2003), further complicated by the inhibition of Hsp90 signaling. It is well accepted that remodeling of the actin cytoskeleton, including changes in tropomyosin, occur in cells undergoing contact guidance (Dalby et al., 2003; Dalby et al., 2008; Gunning et al., 2008). αSMA incorporation into stress fibers stimulated by TGFβ1 via tropomyosin has been demonstrated (Prunotto et al., 2015). Additional studies have demonstrated that geldanamycin treatment can activate stress fiber formation dependent on RhoGTPases and ROCK activity in other cell culture models (Amiri et al., 2007). Together we infer that alignment of stromal cells to the substratum topography is a potent stimulus that acts to modulate stress-fiber formation and αSMA expression regardless of Hsp90 inhibition; however, Hsp90 inhibition was sufficient to promote corneal crystallin expression (*KERA*). That stromal cells retain the ability to form stress fibers is important considering they are essential for remodeling the extracellular matrix during stromal wound repair (Mar et al., 2001). Whether overexpression of *KERA* and αSMA together is beneficial or detrimental, and the mechanisms by which this happens, remains to be seen.

Next, we investigated the ability of 17AAG to modulate KFM transformation as a function of substrate stiffness. We observed that in the presence of 17AAG, on rigid plastic or stiff hydrogels (25 kPa), *KERA* was upregulated while *ACTA2* was inhibited. However, on soft hydrogels (5 kPa) while *KERA* expression was inhibited regardless of TGFβ1 [consistent with (Dreier et al., 2013)] or 17AAG, *ACTA2* expression was significantly greater in the presence of 17AAG while TGFβ1 did not elicit such a potent response. The softer 5 kPa

hydrogels are better mimics of normal corneal tissue stiffness while 25 kPa hydrogels mimic stiffer tissue in rabbits (Dreier et al., 2013; Raghunathan et al., 2017; Thomasy et al., 2014). Together these suggest that Hsp90 inhibition, on substrates that represent 'normal' matrix, potentiate a myofibroblast phenotype.

Since stiffer substrates promoted the keratocyte markers, we next determined whether inhibition of Hsp90 inhibition at a time point when stroma is stiffest (i.e. day 7 (Raghunathan et al., 2017)) would promote wound healing. To do this, we treated rabbit stromal wounds with 17AAG beginning day 7. Once again, we noticed no differences in wound closure between control and 17AAG groups though an elevated rate of re-ulceration persisted. Basement membrane disruption/dissolution often precedes corneal re-ulceration (Matsubara et al., 1991), and re-establishment of an intact basement membrane is critical for stromal repair (Fujikawa et al., 1984; Khodadoust et al., 1968; Laibson, 2010; Santhanam et al., 2017; Torricelli et al., 2016; Torricelli and Wilson, 2014; Torricelli et al., 2013). Coordinated reassembly of the basement membrane is a critical event that triggers the orchestrated localization of junctional proteins to form an intact corneal epithelium (Suzuki et al., 2000). Thus, we lastly determined if 17AAG treatment disrupted a functional epithelial barrier *in vitro*. Indeed, TEER measurements demonstrated significantly lower resistance measurements accompanied with disruption of ZO-1 immunostaining in 17AAG treated stratified corneal epithelial cells suggesting that the barrier integrity is compromised. Whilst this appears to contradict our prior study (Raghunathan et al., 2014) where 17AAG treatment facilitated junction formation, there are key distinctions. First, in the previous study the concentration of 17AAG used was 45 nM compared with 5 or 10 μM here. Second, in the previous study 17AAG promoted junction formation in a monolayer of epithelial cells, while here we showed disruption of barrier function in stratified cells. Lastly, in the previous study our cells were cultured in serum-free defined growth media unlike stratification medium with 10% serum here. These results collectively led us to conclude that a dysregulation in corneal epithelial closure led to disruptions in stromal wound repair with Hsp90 inhibition resulting in increased corneal haze. Lastly, we recognize that the concentration of 17AAG used in our *in vivo* experiments was >10 fold that we used in our *in vitro* experiments and this was dosed either 3 or 6 times daily over the course of 28 or 21 days. The dose chosen was determined from preliminary experiments as the highest tolerated dose. We infer from our study that such a choice of dose may, in hindsight, not be the best approach. Our goal in choosing this dose was to try and maximize our chances of decreasing stromal haze while not incurring negative clinical signs i.e. conjunctival hyperemia, intraocular inflammation, wound healing, etc. Future systematic studies employing a design of experiments (Ferreira et al., 2007) approach may be essential to identify appropriate concentration and time of intervention for 17AAG treatments in future studies. We recognize the importance to determine a balanced dosage that is safe, efficacious and administered at an appropriate time period.

## 5. LIMITATIONS

There are multiple studies which demonstrate the direct translation of Hsp90 inhibition *in vitro* effects with outcomes in experimental models, particularly with significant anti-tumor effects (Menezes et al., 2012; Safavi et al., 2016; Sarkar et al., 2013; Shimamura et al., 2012;

Tran et al., 2010). Therefore, the results obtained *in vivo* were indeed unexpected and stood in stark contrast to our *in vitro* investigations, as the rabbits treated with 17AAG developed more stromal haze than controls irrespective of dose frequency and time to initiation of therapy. The standard pyramid in development of new therapeutics takes in vitro findings with the expectation that it will translate to animal models and ultimately be of benefit to the treatment of human disorders (Horrobin, 2003). It needs to be recognized that the great majority of promising *in vitro* findings fail to translate to successful therapeutics (Bachmann and Ghosh, 2001; Cheung et al., 2009; Hjorth et al., 1985; Rubin, 2002). While the reasons for the discrepant *in vitro* and *in vivo* results remain undefined, there are multiple plausible explanations to help resolve the discordant findings. Firstly, translation of *in vitro* findings to a full organism can be challenging, particularly due to the complexity of the *in vivo* environment. Mixed cell populations assembled to form complex tissues, including epithelial and stromal cells of both the cornea and conjunctiva, have the potential to modulate the host response to treatments. This can either lead to either a dampening or exacerbation of a treatment effects, while other redundant signaling pathways may be enabled *in vivo* that override any effect seen *in vitro*. Secondly, the dosing of 17AAG can be challenging to compare between the *in vitro* and *in vivo* environments. In the current study, the cultured epithelial cells and stromal cells were treated constantly with the drug dissolved in a carrier (DMSO) and constantly present in the culture medium for 24 hours *in vitro*, while there was more of a pulsatile treatment strategy *in vivo* where 17AAG was applied 3-6 times daily with potential peak and trough concentrations within the cornea. Preliminary dose escalation experiments identified the maximum tolerable dose as 100 μM and was thus used in our studies. We did not test the efficacy of 17AAG at lower doses; however, the results from our present study do suggest that a more mechanistic study is required to determine the effects of 17AAG at various doses and various time points for intervention. Further, we did not document the expression levels of Hsp90 (intra- and extracellular) *in situ*. Nevertheless, since geldanamycin compounds suppress TGFβ signaling via Hsp90 inhibition, we documented its effect by analyzing targets of the TGFβ signaling pathway. Additional studies are required to document the mode of action of 17AAG *in vivo*. Additionally, the half-life of 17AAG applied to the ocular surface *in vivo* is unknown, with the potential to reduce its effect if degraded faster when administered topically *in vivo* when compared to treatment of cultured cells *in vitro*. Further studies are required to quantitate the resident times of drugs in the cornea and ocular surface. Lastly, we recognize that the rabbits used in this study were relatively young (3-4 months old) animals. Thus their responses to the frequent dosing or response to drugs may differ from adult animals. While rabbits this age are commonly used for pre-clinical evaluation, additional studies are required to document the effect of age.

## 6. CONCLUSIONS

In conclusion, we demonstrate comprehensively using *in vitro* and *in vivo* approaches that Hsp90 inhibition successfully promotes reverse transformation of myofibroblasts to a keratocyte phenotype on rigid / stiff substrates *in vitro*. However, on substrates mimicking normal or softer corneas this is not true. Thus, screening of drug candidates for corneal wound healing should be performed employing biologically relevant substrates. Using an *in*

*vivo* PTK model in rabbit, we demonstrate that elevated doses of an Hsp90 inhibitor may cause recurrent corneal erosions with persistent haze. Lastly, we show that Hsp90 inhibition may break the epithelial barrier integrity; whether such a strategy may be used to promote epithelial permeability to deliver drugs to the stroma warrants further investigations.

## Supplementary Material

Refer to Web version on PubMed Central for supplementary material.

## ACKNOWLEDGMENTS

We would like to thank Monica J Motta and the undergraduate student team ('A-team') for help with handling the animals through the duration of the project. This study was supported by grants from the National Eye Institute (R01EY016134, R01EY019970, K08EY021142, K08EY028199, P30EY12576), ACVO- Vison for Animals Foundation VAF2015-01, and Center for Companion Animal Health (SVM-UC Davis). VKR was also supported partially by start-up funds at UHCO.

## REFERENCES

Amiri A, Noei F, Feroz T, Lee JM, 2007 Geldanamycin Anisimycins Activate Rho and Stimulate Rho- and ROCK-Dependent Actin Stress Fiber Formation. Mol. Cancer Res 5, 933–942. [PubMed: 17855662]

Andersson A-S, Olsson P, Lidberg U, Sutherland D, 2003 The effects of continuous and discontinuous groove edges on cell shape and alignment. Exp. Cell Res 288, 177–188. [PubMed: 12878169]

Argüeso P, Gipson IK, 2012 Assessing mucin expression and function in human ocular surface epithelia in vivo and in vitro, in: McGuckin M, Thornton D (Eds.), Mucins. Methods and Protocols. Springer, pp. 313–325.

Au HT, Cheng I, Chowdhury MF, Radisic M, 2007 Interactive effects of surface topography and pulsatile electrical field stimulation on orientation and elongation of fibroblasts and cardiomyocytes. Biomaterials 28, 4277–4293. [PubMed: 17604100]

Bachmann KA, Ghosh R, 2001 The use of in vitro methods to predict in vivo pharmacokinetics and drug interactions. Curr Drug Metab 2, 299–314. [PubMed: 11513332]

Cheung AL, Yang SJ, Bayer AS, Xiong YQ, 2009 Disparity in the in vitro versus in vivo regulation of fibronectin-binding proteins by 2 global regulators, saeRS and sigB, in Staphylococcus aureus. J Infect Dis 200, 1371–1374. [PubMed: 19807278]

Czar MJ, Welsh MJ, Pratt WB, 1996 Immunofluorescence localization of the 90-kDa heat-shock protein to cytoskeleton. Eur. J. Cell Biol 70, 322–330. [PubMed: 8864660]

Dalby MJ, Childs S, Riehle MO, Johnstone HJ, Affrossman S, Curtis AS, 2003 Fibroblast reaction to island topography: changes in cytoskeleton and morphology with time. Biomaterials 24, 927–935. [PubMed: 12504513]

Dalby MJ, Hart A, Yarwood SJ, 2008 The effect of the RACK1 signalling protein on the regulation of cell adhesion and cell contact guidance on nanometric grooves. Biomaterials 29, 282–289. [PubMed: 17936896]

de Medeiros FW, Mohan RR, Suto C, Sinha S, Bonilha VL, Chaurasia SS, Wilson SE, 2008 Haze development after photorefractive keratectomy: mechanical vs ethanol epithelial removal in rabbits. J. Refract. Surg 24, 923–927. [PubMed: 19044233]

Dreier B, Raghunathan V, Russell P, Murphy CJ, 2012 Involvement Of Yap And TAZ In The Response Of Corneal Cells To Biophysical Cues. ARVO Meeting Abstracts 53, 4202.

Dreier B, Thomasy SM, Mendonsa R, Raghunathan VK, Russell P, Murphy CJ, 2013 Substratum compliance modulates corneal fibroblast to myofibroblast transformation. Invest. Ophthalmol. Vis. Sci 54, 5901–5907. [PubMed: 23860754]

Eaton JS, Miller PE, Bentley E, Thomasy SM, Murphy CJ, 2017 The SPOTS System: An Ocular Scoring System Optimized for Use in Modern Preclinical Drug Development and Toxicology. J. Ocul. Pharmacol. Ther 33, 718–734. [PubMed: 29239680]

Ferreira SLC, Bruns RE, Ferreira HS, Matos GD, David JM, Brandão GC, da Silva EGP, Portugal LA, dos Reis PS, Souza AS, dos Santos WNL, 2007 Box-Behnken design: An alternative for the optimization of analytical methods. Anal. Chim. Acta 597, 179–186. [PubMed: 17683728]

Fini ME, 1999 Keratocyte and fibroblast phenotypes in the repairing cornea. Prog. Retin. Eye Res 18, 529–551. [PubMed: 10217482]

Folger PA, Zekaria D, Grotendorst G, Masur SK, 2001 Transforming Growth Factory-β–Stimulated Connective Tissue Growth Factor Expression during Corneal Myofibroblast Differentiation. Invest. Ophthalmol. Vis. Sci 42, 2534–2541. [PubMed: 11581194]

Fraser SA, Ting YH, Mallon KS, Wendt AE, Murphy CJ, Nealey PF, 2008 Submicron and nanoscale feature depth modulates alignment of stromal fibroblasts and corneal epithelial cells in serum-rich and serum-free media. J. Biomed. Mater. Res. A 86, 725–735. [PubMed: 18041718]

Fujikawa LS, Foster CS, Gipson IK, Colvin RB, 1984 Basement membrane components in healing rabbit corneal epithelial wounds: immunofluorescence and ultrastructural studies. The Journal of Cell Biology 98, 128–138. [PubMed: 6368566]

Funderburgh JL, Funderburgh ML, Mann MM, Corpuz L, Roth MR, 2001 Proteoglycan Expression during Transforming Growth Factor β-induced Keratocyte-Myofibroblast Transdifferentiation. J. Biol. Chem 276, 44173–44178. [PubMed: 11555658]

Grenert JP, Johnson BD, Toft DO, 1999 The importance of ATP binding and hydrolysis by hsp90 in formation and function of protein heterocomplexes. J. Biol. Chem 274, 17525–17533. [PubMed: 10364185]

Grenert JP, Sullivan WP, Fadden P, Haystead TAJ, Clark J, Mimnaugh E, Krutzsch H, Ochel H-J, Schulte TW, Sausville E, Neckers LM, Toft DO, 1997 The Amino-terminal Domain of Heat Shock Protein 90 (hsp90) That Binds Geldanamycin Is an ATP/ADP Switch Domain That Regulates hsp90 Conformation. J. Biol. Chem 272, 23843–23850. [PubMed: 9295332]

Grinnell F, Petroll WM, 2010 Cell motility and mechanics in three-dimensional collagen matrices. Annu. Rev. Cell. Dev. Biol 26, 335–361. [PubMed: 19575667]

Gunning P, O'neill G, Hardeman E, 2008 Tropomyosin-Based Regulation of the Actin Cytoskeleton in Time and Space. Physiol. Rev 88, 1–35. [PubMed: 18195081]

Hjorth S, Clark D, Carlsson A, 1985 Lack of functional evidence for the involvement of sigma opiate receptors in the actions of the 3-PPP enantiomers on central dopaminergic systems: discrepancies between in vitro and in vivo observations. Life Sci 37, 673–684. [PubMed: 2410756]

Horrobin DF, 2003 Modern biomedical research: an internally self-consistent universe with little contact with medical reality? Nat Rev Drug Discov 2, 151–154. [PubMed: 12563306]

Hu B, Wu Z, Phan SH, 2003 Smad3 mediates transforming growth factor-beta-induced alpha-smooth muscle actin expression. Am J Respir Cell Mol Biol 29, 397–404. [PubMed: 12702545]

Jayaprakash P, Dong H, Zou M, Bhatia A, O'Brien K, Chen M, Woodley DT, Li W, 2015 Hsp90alpha and Hsp90beta Co-Operate a Stress-Response Mechanism to Cope With Hypoxia and Nutrient Paucity during Wound Healing. J. Cell Sci

Jester JV, Brown D, Pappa A, Vasiliou V, 2012 Myofibroblast differentiation modulates keratocyte crystallin protein expression, concentration, and cellular light scattering. Invest. Ophthalmol. Vis. Sci 53, 770–778. [PubMed: 22247459]

Jester JV, Huang J, Barry-Lane PA, Kao WWY, Petroll WM, Cavanagh HD, 1999 Transforming growth factory(β)-mediated corneal myofibroblast differentiation requires actin and fibronectin assembly. Invest. Ophthalmol. Vis. Sci 40, 1959–1967. [PubMed: 10440249]

Karamichos D, Lakshman N, Petroll WM, 2007 Regulation of Corneal Fibroblast Morphology and Collagen Reorganization by Extracellular Matrix Mechanical Properties. Invest. Ophthalmol. Vis. Sci 48, 5030–5037. [PubMed: 17962454]

Karuri NW, Liliensiek S, Teixeira AI, Abrams G, Campbell S, Nealey PF, Murphy CJ, 2004 Biological length scale topography enhances cell-substratum adhesion of human corneal epithelial cells. J. Cell Sci 117, 3153–3164. [PubMed: 15226393]

Karuri NW, Porri TJ, Albrecht RM, Murphy CJ, Nealey PF, 2006 Nano- and microscale holes modulate cell-substrate adhesion, cytoskeletal organization, and -beta1 integrin localization in SV40 human corneal epithelial cells. IEEE Trans Nanobioscience 5, 273–280. [PubMed: 17181027]

Kaur H, Chaurasia SS, Agrawal V, Suto C, Wilson SE, 2009 Corneal myofibroblast viability: Opposing effects of IL-1 and TGF β1. Exp. Eye Res 89, 152–158. [PubMed: 19285499]

Khodadoust A, Silverstein A, Kenyon D, Dowling J, 1968 Adhesion of regenerating corneal epithelium. The role of basement membrane. Am. J. Ophthalmol 65, 339. [PubMed: 5640539]

Kim S, Gates BL, Leonard BC, Gragg MM, Pinkerton KE, Van Winkle LS, Murphy CJ, Pyrgiotakis G, Zhang Z, Demokritou P, Thomasy SM, 2020 Engineered metal oxide nanomaterials inhibit corneal epithelial wound healing in vitro and in vivo. NanoImpact 17, 100198. [PubMed: 32154443]

Kirschke E, Goswami D, Southworth D, Griffin, Patrick R, Agard, David A, 2014 Glucocorticoid Receptor Function Regulated by Coordinated Action of the Hsp90 and Hsp70 Chaperone Cycles. Cell 157, 1685–1697. [PubMed: 24949977]

Kivanany P, Grose K, Yonet-Tanyeri N, Manohar S, Sunkara Y, Lam K, Schmidtke D, Varner V, Petroll W, 2018 An In Vitro Model for Assessing Corneal Keratocyte Spreading and Migration on Aligned Fibrillar Collagen. Journal of Functional Biomaterials 9, 54.

Laibson PR, 2010 Recurrent Corneal Erosions and Epithelial Basement Membrane Dystrophy. Eye & Contact Lens 36, 315–317 310.1097/ICL.1090b1013e3181f1018ff1097. [PubMed: 20724847]

Lakshman N, Petroll WM, 2012 Growth factor regulation of corneal keratocyte mechanical phenotypes in 3-D collagen matrices. Invest. Ophthalmol. Vis. Sci 53, 1077–1086. [PubMed: 22247479]

Liliensiek SJ, Campbell S, Nealey PF, Murphy CJ, 2006 The scale of substratum topographic features modulates proliferation of corneal epithelial cells and corneal fibroblasts. J. Biomed. Mater. Res. A 79, 185–192. [PubMed: 16817223]

Mar PK, Roy P, Yin HL, Cavanagh HD, Jester JV, 2001 Stress fiber formation is required for matrix reorganization in a corneal myofibroblast cell line. Exp. Eye Res 72, 455–466. [PubMed: 11273673]

Matsubara M, Zieske JD, Fini ME, 1991 Mechanism of basement membrane dissolution preceding corneal ulceration. Invest. Ophthalmol. Vis. Sci 32, 3221–3237. [PubMed: 1660857]

Menezes DL, Taverna P, Jensen MR, Abrams T, Stuart D, Yu GK, Duhl D, Machajewski T, Sellers WR, Pryer NK, Gao Z, 2012 The novel oral Hsp90 inhibitor NVP-HSP990 exhibits potent and broad-spectrum antitumor activities in vitro and in vivo. Mol Cancer Ther 11, 730–739. [PubMed: 22246440]

Mosmann T, 1983 Rapid colorimetric assay for cellular growth and survival: application to proliferation and cytotoxicity assays. J. Immunol. Methods 65, 55. [PubMed: 6606682]

Myrna KE, Mendonsa R, Russell P, Pot SA, Liliensiek SJ, Jester JV, Nealey PF, Brown D, Murphy CJ, 2012 Substratum topography modulates corneal fibroblast to myofibroblast transformation. Invest. Ophthalmol. Vis. Sci 53, 811–816. [PubMed: 22232431]

Netto MV, Mohan RR, Sinha S, Sharma A, Dupps W, Wilson SE, 2006 Stromal haze, myofibroblasts, and surface irregularity after PRK. Exp. Eye Res 82, 788–797. [PubMed: 16303127]

Noh H, Kim HJ, Yu MR, Kim W-Y, Kim J, Ryu JH, Kwon SH, Jeon JS, Han DC, Ziyadeh F, 2012 Heat shock protein 90 inhibitor attenuates renal fibrosis through degradation of transforming growth factor-[beta] type II receptor. Lab. Invest 92, 1583–1596. [PubMed: 22964853]

Park SA, Covert J, Teixeira L, Motta MJ, DeRemer SL, Abbott NL, Dubielzig R, Schurr M, Isseroff RR, McAnulty JF, Murphy CJ, 2015 Importance of defining experimental conditions in a mouse excisional wound model. Wound Repair Regen. 23, 251–261. [PubMed: 25703258]

Pearl LH, Prodromou C, 2006 Structure and mechanism of the Hsp90 molecular chaperone machinery. Annu. Rev. Biochem 75, 271–294. [PubMed: 16756493]

Petroll WM, Kivanany PB, Hagenasr D, Graham EK, 2015 Corneal Fibroblast Migration Patterns During Intrastromal Wound Healing Correlate With ECM Structure and AlignmentFibroblast Patterning During Intrastromal Migration. Invest. Ophthalmol. Vis. Sci 56, 7352–7361. [PubMed: 26562169]

Petroll WM, Lakshman N, 2015 Fibroblastic Transformation of Corneal Keratocytes by Rac Inhibition is Modulated by Extracellular Matrix Structure and Stiffness. J Funct Biomater 6, 222–240. [PubMed: 25874856]

Petroll WM, Miron-Mendoza M, 2015 Mechanical interactions and crosstalk between corneal keratocytes and the extracellular matrix. Exp. Eye Res 133, 49–57. [PubMed: 25819454]

Pot SA, Liliensiek SJ, Myrna KE, Bentley E, Jester JV, Nealey PF, Murphy CJ, 2010 Nanoscale topography-induced modulation of fundamental cell behaviors of rabbit corneal keratocytes, fibroblasts, and myofibroblasts. Invest. Ophthalmol. Vis. Sci 51, 1373–1381. [PubMed: 19875665]

Pratt WB, Toft DO, 2003 Regulation of signaling protein function and trafficking by the hsp90/hsp70-based chaperone machinery. Exp. Biol. Med. (Maywood) 228, 111–133. [PubMed: 12563018]

Prunotto M, Bruschi M, Gunning P, Gabbiani G, Weibel F, Ghiggeri GM, Petretto A, Scaloni A, Bonello T, Schevzov G, Alieva I, Bochaton-Piallat ML, Candiano G, Dugina V, Chaponnier C, 2015 Stable incorporation of alpha-smooth muscle actin into stress fibers is dependent on specific tropomyosin isoforms. Cytoskeleton (Hoboken) 72, 257–267. [PubMed: 26147585]

Raghunathan VK, Dreier B, Morgan JT, Tuyen BC, Rose BW, Reilly CM, Russell P, Murphy CJ, 2014 Involvement of YAP, TAZ and HSP90 in contact guidance and intercellular junction formation in corneal epithelial cells. PLoS One 9, e109811. [PubMed: 25290150]

Raghunathan VK, Morgan JT, Dreier B, Reilly CM, Thomasy SM, Wood JA, Ly I, Tuyen BC, Hughbanks M, Murphy CJ, Russell P, 2013 Role of substratum stiffness in modulating genes associated with extracellular matrix and mechanotransducers YAP and TAZ. Invest. Ophthalmol. Vis. Sci 54, 378–386. [PubMed: 23258147]

Raghunathan VK, Thomasy SM, Strom P, Yanez-Soto B, Garland SP, Sermeno J, Reilly CM, Murphy CJ, 2017 Tissue and cellular biomechanics during corneal wound injury and repair. Acta Biomater. 58, 291–301. [PubMed: 28559158]

Robertson DM, Li L, Fisher S, Pearce VP, Shay JW, Wright WE, Cavanagh HD, Jester JV, 2005 Characterization of Growth and Differentiation in a Telomerase-Immortalized Human Corneal Epithelial Cell Line. Invest. Ophthalmol. Vis. Sci 46, 470–478. [PubMed: 15671271]

Roe SM, Prodromou C, O'Brien R, Ladbury JE, Piper PW, Pearl LH, 1999 Structural Basis for Inhibition of the Hsp90 Molecular Chaperone by the Antitumor Antibiotics Radicicol and Geldanamycin. J. Med. Chem 42, 260–266. [PubMed: 9925731]

Rubin H, 2002 The disparity between human cell senescence in vitro and lifelong replication in vivo. Nat Biotechnol 20, 675–681. [PubMed: 12089551]

Safavi S, Jarnum S, Vannas C, Udhane S, Jonasson E, Tomic TT, Grundevik P, Fagman H, Hansson M, Kalender Z, Jauhiainen A, Dolatabadi S, Stratford EW, Myklebost O, Eriksson M, Stenman G, Schneider-Stock R, Stahlberg A, Aman P, 2016 HSP90 inhibition blocks ERBB3 and RET phosphorylation in myxoid/round cell liposarcoma and causes massive cell death in vitro and in vivo. Oncotarget 7, 433–445. [PubMed: 26595521]

Sakamoto T, Ueno H, Sonoda K, Hisatomi T, Shimizu K, Ohashi H, Inomata H, 2000 Blockade of TGF-beta by in vivo gene transfer of a soluble TGF-beta type II receptor in the muscle inhibits corneal opacification, edema and angiogenesis. Gene Ther. 7, 1915–1924. [PubMed: 11127579]

Santhanam A, Marino GK, Torricelli AA, Wilson SE, 2017 EBM regeneration and changes in EBM component mRNA expression in stromal cells after corneal injury. Mol. Vis 23, 39–51. [PubMed: 28275314]

Sarkar S, Dutta D, Samanta SK, Bhattacharya K, Pal BC, Li J, Datta K, Mandal C, Mandal C, 2013 Oxidative inhibition of Hsp90 disrupts the super-chaperone complex and attenuates pancreatic adenocarcinoma in vitro and in vivo. Int J Cancer 132, 695–706. [PubMed: 22729780]

Shimamura T, Perera SA, Foley KP, Sang J, Rodig SJ, Inoue T, Chen L, Li D, Carretero J, Li YC, Sinha P, Carey CD, Borgman CL, Jimenez JP, Meyerson M, Ying W, Barsoum J, Wong KK, Shapiro GI, 2012 Ganetespib (STA-9090), a nongeldanamycin HSP90 inhibitor, has potent antitumor activity in in vitro and in vivo models of non-small cell lung cancer. Clin Cancer Res 18, 4973–4985. [PubMed: 22806877]

Stramer BM, Cook JR, Fini ME, Taylor A, Obin M, 2001 Induction of the ubiquitin-proteasome pathway during the keratocyte transition to the repair fibroblast phenotype. Invest. Ophthalmol. Vis. Sci 42, 1698–1706. [PubMed: 11431431]

Stramer BM, Fini ME, 2004 Uncoupling keratocyte loss of corneal crystallin from markers of fibrotic repair. Invest. Ophthalmol. Vis. Sci 45, 4010–4015. [PubMed: 15505050]

Suzuki K, Tanaka T, Enoki M, Nishida T, 2000 Coordinated reassembly of the basement membrane and junctional proteins during corneal epithelial wound healing. Invest. Ophthalmol. Vis. Sci 41, 2495–2500. [PubMed: 10937559]

Tabdanov ED, Puram V, Zhovmer A, Provenzano PP, 2018 Microtubule-Actomyosin Mechanical Cooperation during Contact Guidance Sensing. Cell Rep 25, 328–338 e326. [PubMed: 30304674]

Tandon A, Tovey JC, Sharma A, Gupta R, Mohan RR, 2010 Role of transforming growth factor Beta in corneal function, biology and pathology. Curr. Mol. Med 10, 565–578. [PubMed: 20642439]

Teixeira AI, Abrams GA, Bertics PJ, Murphy CJ, Nealey PF, 2003 Epithelial contact guidance on well-defined micro- and nanostructured substrates. J. Cell Sci 116, 1881–1892. [PubMed: 12692189]

Thomasy SM, Raghunathan VK, Miyagi H, Evashenk AT, Sermeno JC, Tripp GK, Morgan JT, Murphy CJ, 2018 Latrunculin B and substratum stiffness regulate corneal fibroblast to myofibroblast transformation. Exp. Eye Res 170, 101–107. [PubMed: 29421383]

Thomasy SM, Raghunathan VK, Winkler M, Reilly CM, Sadeli AR, Russell P, Jester JV, Murphy CJ, 2014 Elastic modulus and collagen organization of the rabbit cornea: epithelium to endothelium. Acta Biomater. 10, 785–791. [PubMed: 24084333]

Tocce EJ, Smirnov VK, Kibalov DS, Liliensiek SJ, Murphy CJ, Nealey PF, 2010 The ability of corneal epithelial cells to recognize high aspect ratio nanostructures. Biomaterials 31, 4064–4072. [PubMed: 20153044]

Tomcik M, Zerr P, Pitkowski J, Palumbo-Zerr K, Avouac J, Distler O, Becvar R, Senolt L, Schett G, Distler JH, 2014 Heat shock protein 90 (Hsp90) inhibition targets canonical TGF-beta signalling to prevent fibrosis. Ann. Rheum. Dis 73, 1215–1222. [PubMed: 23661493]

Torricelli AA, Santhanam A, Wu J, Singh V, Wilson SE, 2016 The corneal fibrosis response to epithelial-stromal injury. Exp. Eye Res 142, 110–118. [PubMed: 26675407]

Torricelli AA, Wilson SE, 2014 Cellular and extracellular matrix modulation of corneal stromal opacity. Exp. Eye Res 129, 151–160. [PubMed: 25281830]

Torricelli AAM, Singh V, Santhiago MR, Wilson SE, 2013 The Corneal Epithelial Basement Membrane: Structure, Function, and Disease. Invest. Ophthalmol. Vis. Sci 54, 6390–6400. [PubMed: 24078382]

Tran PL, Kim SA, Choi HS, Yoon JH, Ahn SG, 2010 Epigallocatechin-3-gallate suppresses the expression of HSP70 and HSP90 and exhibits anti-tumor activity in vitro and in vivo. BMC Cancer 10, 276. [PubMed: 20537126]

van Setten G, Schultz G, 1994 Transforming growth factor-alpha is a constant component of human tear fluid. Graefes Arch. Clin. Exp. Ophthalmol 232, 523–526. [PubMed: 7959090]

Wilson SE, 2002 Analysis of the keratocyte apoptosis, keratocyte proliferation, and myofibroblast transformation responses after photorefractive keratectomy and laser in situ keratomileusis. Trans. Am. Ophthalmol. Soc 100, 411–433. [PubMed: 12545703]

Wilson SE, He YG, Weng J, Zieske JD, Jester JV, Schultz GS, 1994 Effect of epidermal growth factor, hepatocyte growth factor, and keratinocyte growth factor, on proliferation, motility and differentiation of human corneal epithelial cells. Exp. Eye Res 59, 665–678. [PubMed: 7698260]

Wood JA, Shah NM, McKee CT, Hughbanks ML, Liliensiek SJ, Russell P, Murphy CJ, 2011 The role of substratum compliance of hydrogels on vascular endothelial cell behavior. Biomaterials 32, 5056–5064. [PubMed: 21501863]

Wrighton KH, Lin X, Feng XH, 2008 Critical regulation of TGFbeta signaling by Hsp90. Proc. Natl. Acad. Sci. U. S. A 105, 9244–9249. [PubMed: 18591668]

Xu M, Dittmar KD, Giannoukos G, Pratt WB, Simons SS, 1998 Binding of hsp90 to the Glucocorticoid Receptor Requires a Specific 7-Amino Acid Sequence at the Amino Terminus of the Hormone-binding Domain. J. Biol. Chem 273, 13918–13924. [PubMed: 9593740]

Yanez-Soto B, Leonard BC, Raghunathan VK, Abbott NL, Murphy CJ, 2015 Effect of Stratification on Surface Properties of Corneal Epithelial Cells. Invest. Ophthalmol. Vis. Sci 56, 8340–8348. [PubMed: 26747762]

Zhang X, Clark AF, Yorio T, 2006 Heat Shock Protein 90 Is an Essential Molecular Chaperone for Nuclear Transport of Glucocorticoid Receptor β. Invest. Ophthalmol. Vis. Sci 47, 700–708. [PubMed: 16431970]

Zi Z, Chapnick DA, Liu X, 2012 Dynamics of TGF-beta/Smad signaling. FEBS Lett 586, 1921–1928. [PubMed: 22710166]

## Highlights

- Hsp90 inhibition facilitates retention of keratocyte phenotype regardless of TGFβ stimulus on rigid substrates and stiff hydrogels *in vitro*.
- On softer hydrogels, or anisotropically patterned topography, Hsp90 inhibition promotes retension of myofibroblasts phenotype *in vitro*.
- *In vivo*, Hsp90 inhibition did not significantly modulate wound repair although recurrent corneal epithelial defects were observed.
- *In vitro*, Hsp90 inhibition resulted in disruption of epithelial barrier integrity with little toxicity.

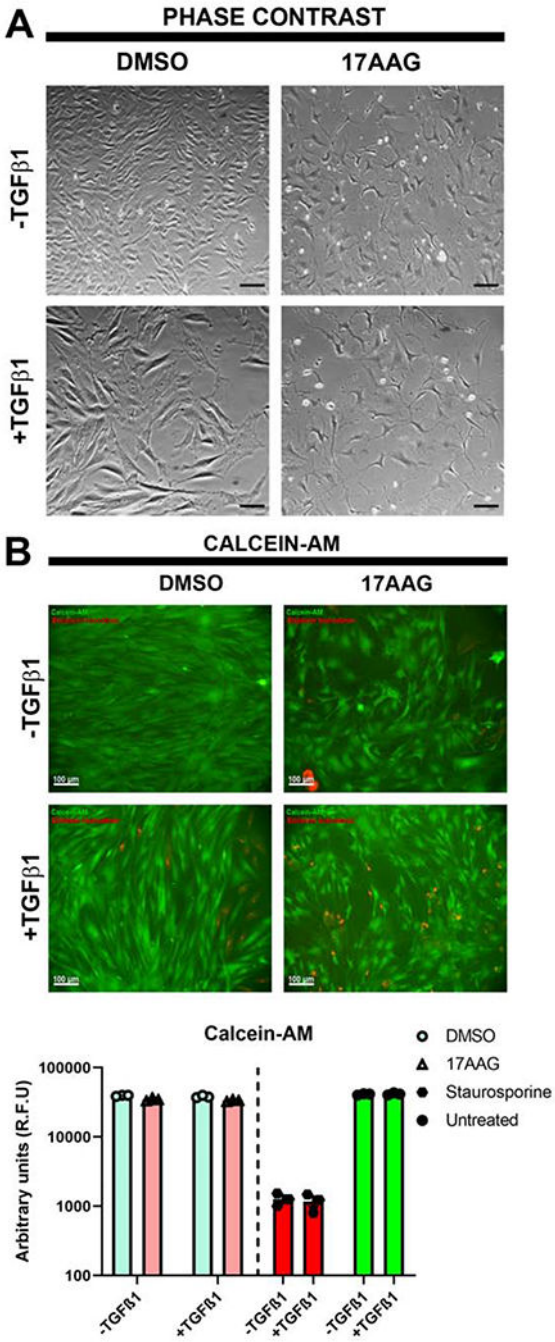


**Figure 1: Hsp90 inhibition alters stromal cell morphology without altering viability.**

**(A)** Phase contrast images demonstrate a change in cell morphology from spindle shaped fibroblast/myofibroblasts to stellate/dendritic keratocyte-like with 500 nM 17AAG treatment in the presence/absence of 10 ng/ml TGFβ1 treatment. Scale bar is 100 μm. **(B)** Calcein-AM/ethidium homodimer labelling demonstrates that 500 nM 17AAG did not detrimentally affect cell viability. Scale bar is 100 μm. Staurosporine was used as positive control for loss of cell viability while untreated cells were negative control. Images are representative ones

observed from three independent experiments. Histograms are data from n =3 independent experiments, with mean ± standard deviation.

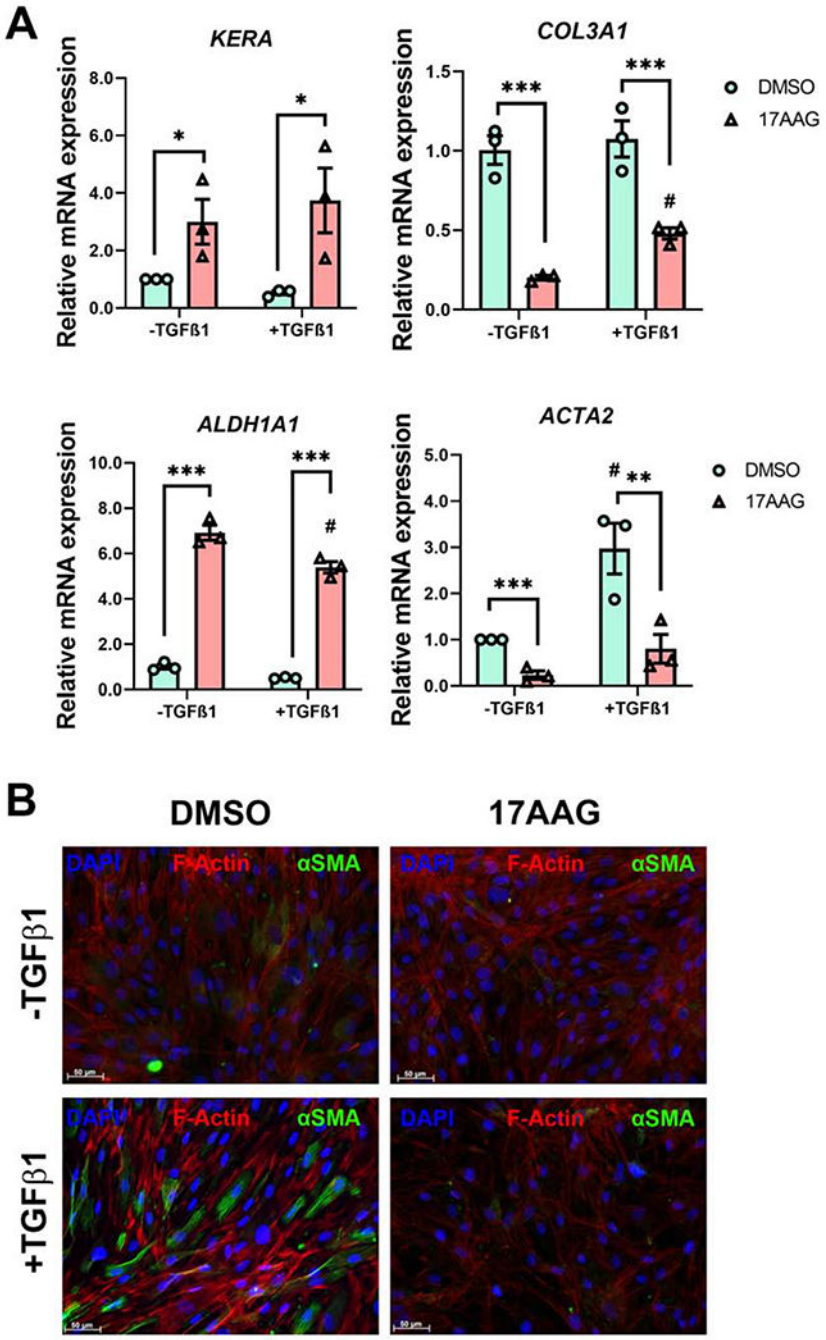


**Figure 2: Hsp90 inhibition upregulates keratocyte markers while suppressing myofibroblast markers *in vitro*.**

**(A)** Relative mRNA expression of keratocan (*KERA*), collagen 3A1 (*COL3A1*), aldehyde dehydrogenase 1A1 (*ALDH1A1*) and αSMA (*ACTA2*) by rabbit corneal stromal cells treated with DMSO (vehicle control) or 500 nM 17AAG in the presence/absence of 10 ng/ml TGFβ1 for 3 days. **(B)** Representative fluorescence images of RCFs immunolabelled for expression of αSMA, F-actin, and counterstained with DAPI. Images are representative of three independent experiments. Bar plots represent data expressed as mean ± standard

error in mean (SEM) along with individual data points from n = 3 independent experiments. Two-way ANOVA followed by Tukey's multiple comparisons was performed to establish statistical significance. *p<0.05, **p<0.01, ***p<0.001 compared with DMSO control. #p<0.05 comparing +TGFβ1 with −TGFβ1 cells within the same treatment group (i.e. 17AAG vs DMSO).

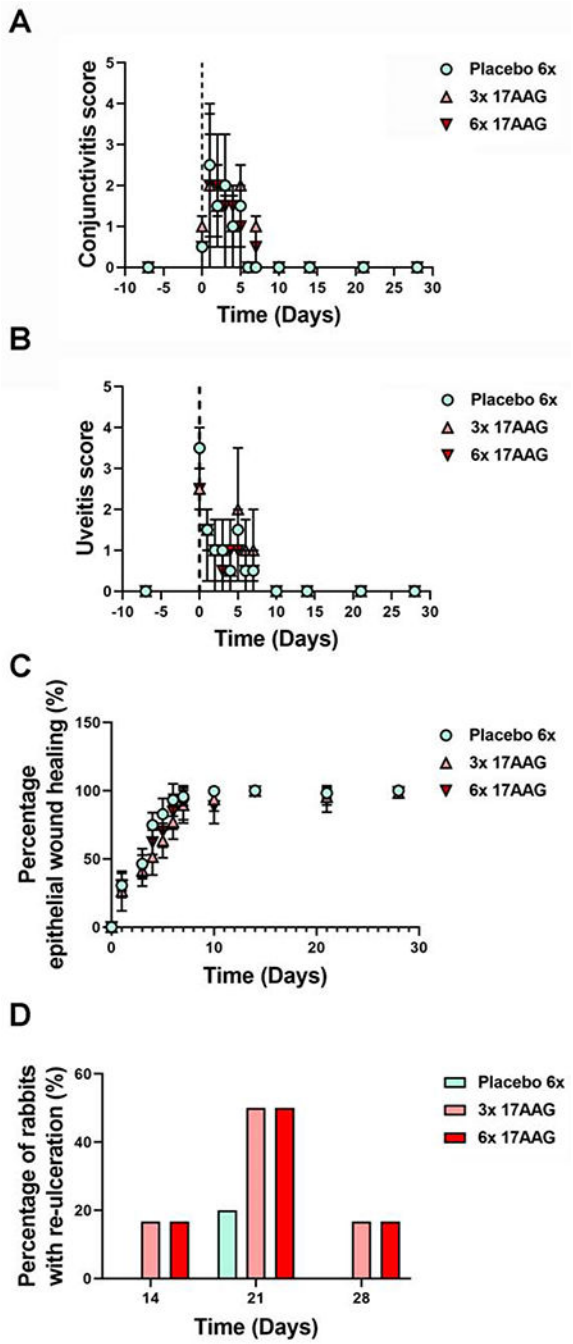


**Figure 3: Hsp90 inhibition immediately after PTK wounding does not improve stromal wound healing.**

**(A)** Conjunctivitis score determined by the presence of conjunctival congestion, chemosis and discharge, **(B),** Uveitis score determined by the presence of aqueous flare, anterior chamber cell and iridal hyperemia **(C),** percentage epithelial wound healing determined by the quantitative assessment of fluorescein staining in the PTK treated eye, and **(D)** percentage of rabbits with epithelial re-ulceration over 28 days. Data are mean ± standard deviation from n = 6 animals.

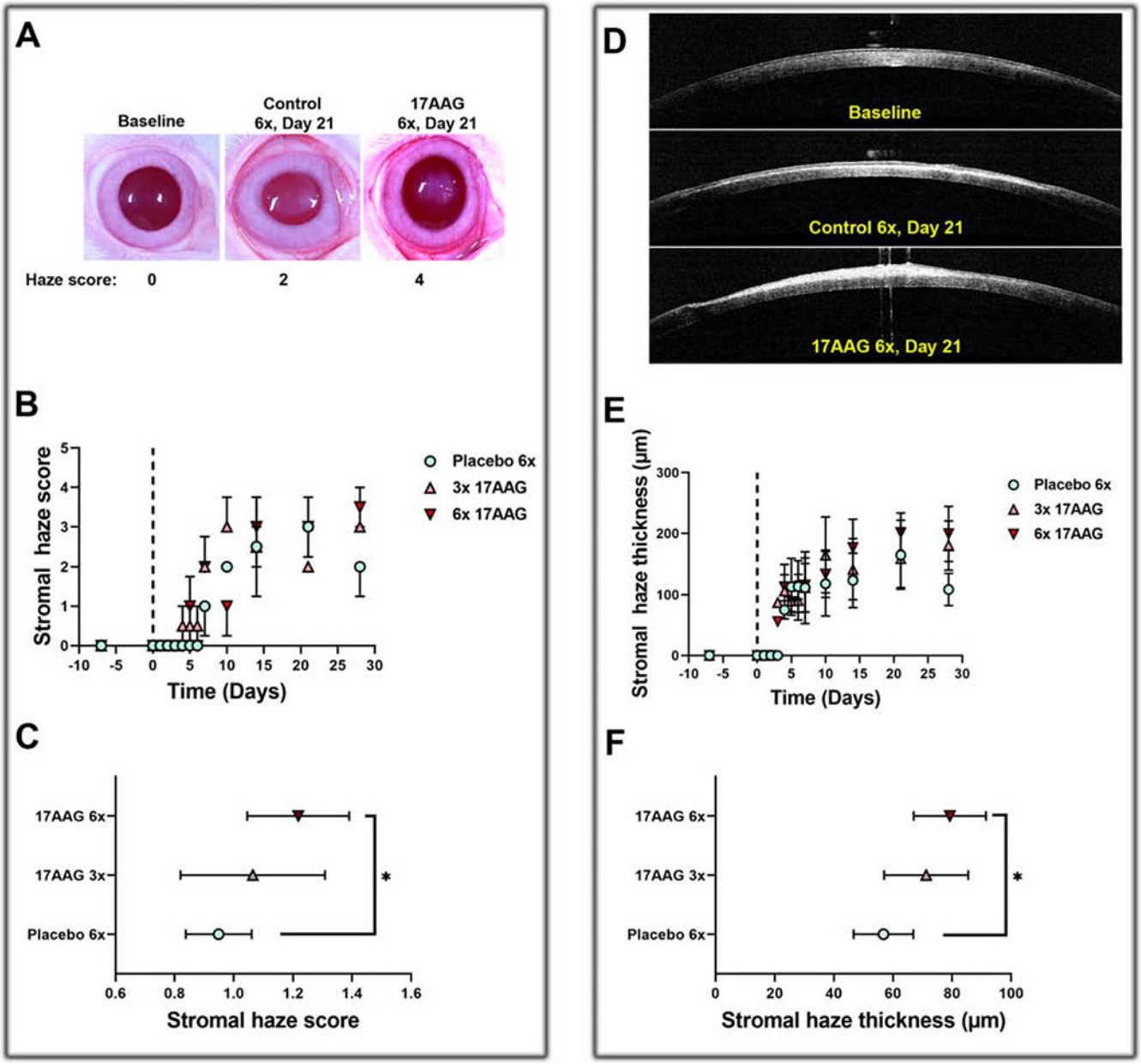


**Figure 4: Hsp90 inhibition immediately after PTK wounding results in increased stromal haze formation.**

**(A)** Representative clinical images demonstrating stromal haze in both control and 17AAG treated groups when compared with baseline, **(B)** stromal haze scoring using the SPOTs system in rabbits over the course of treatment, **(C)** average stromal haze score as a function of treatment, and **(D)** representative long axis lens views of the central cornea taken at baseline and Day 21 in both control and 17AAG treated rabbits demonstrated a thickened band of hyperreflective section in the anterior stroma consistent with clinical stromal haze formation, **(E)** Quantitative analysis of the stromal haze documented using FD-OCT over time in control and 17AAG treated rabbits, **(F)** Average stromal haze thickness as a function of treatment group, are illustrated. Data are mean ± standard deviation from n = 6 animals.

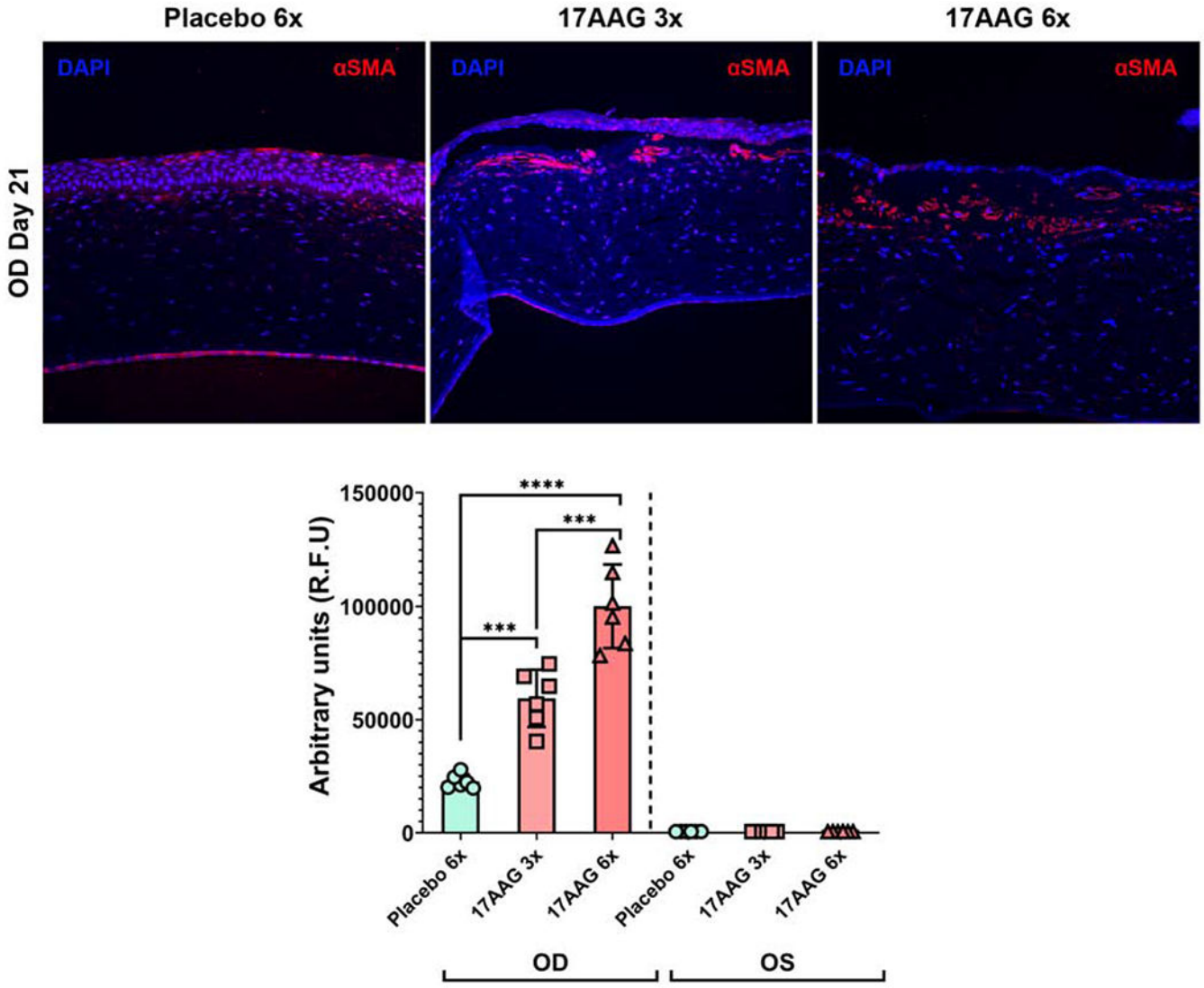


**Figure 5: Hsp90 inhibition results in increased immunostaining of αSMA positive stromal cells.**

Representative immunohistochemistry images from rabbit cornea on day 21, after PTK wounding, demonstrating the incidence of myofibroblasts (αSMA staining, red) in control and 17AAG treated animals. Nuclei are stained with DAPI (blue) Bar plot demonstrates mean ± standard deviation of relative fluorescence intensity quantified for αSMA immunolabel from n = 6 animals per group. One-way ANOVA followed by Tukey's multiple comparison test was performed to establish statistical significance. ***p<0.001, ****p<0.0001 compared respective groups indicated.

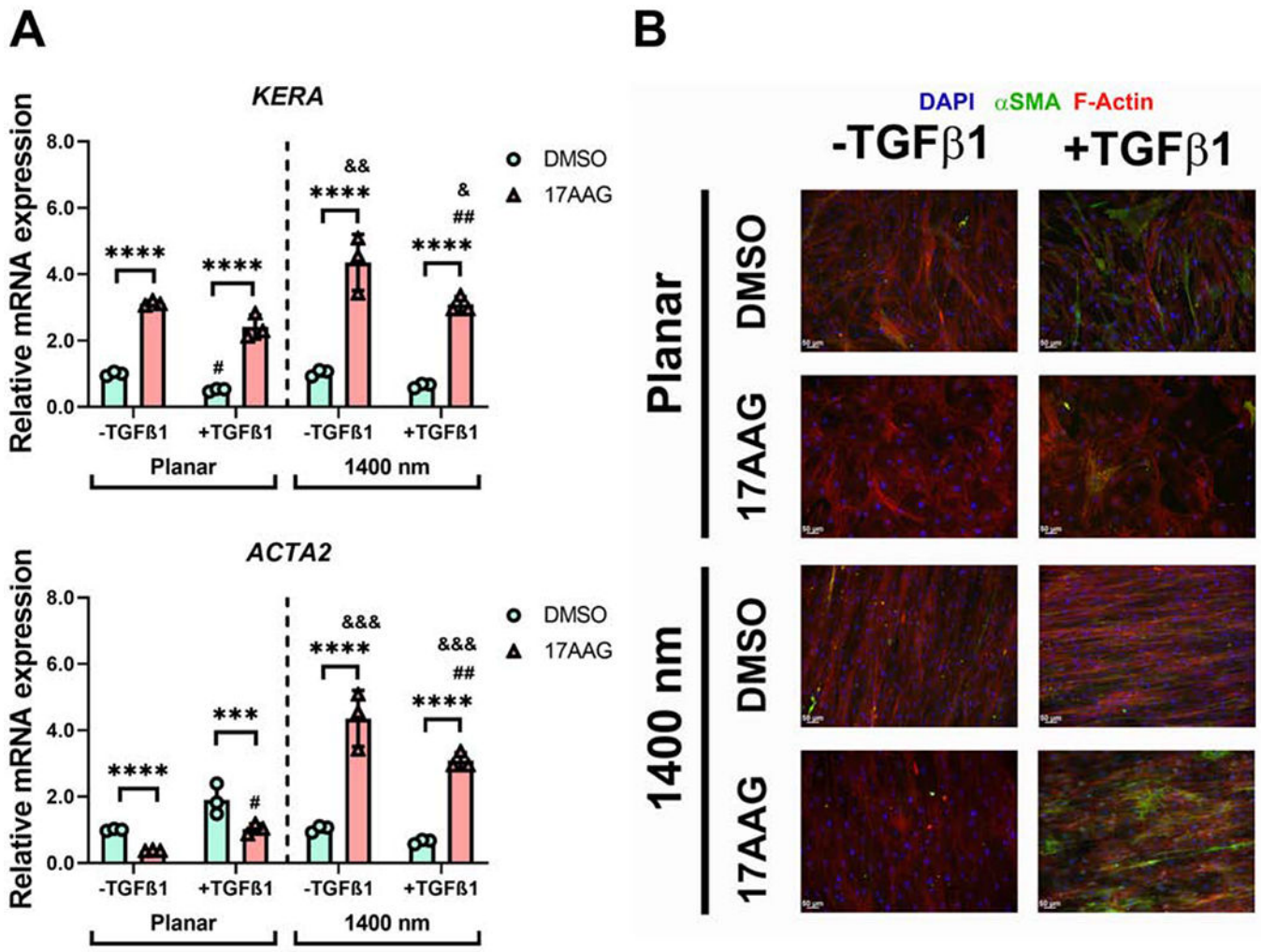


**Figure 6: Substratum topography modulates cellular response to Hsp90 inhibition and TGFβ1 treatment.**

**(A)** Relative mRNA expression for *KERA* and *ACTA2* by RCFs cultured on either planar or 1400 nm pitch anisotropically patterned substrates and treated with DMSO (vehicle control) or 500 nM 17AAG in the presence/absence of 10 ng/ml TGFβ1 for 3 days. **(B)** Representative immunocytochemistry image demonstrating immunolabeling for αSMA (green), F-Actin (red), and DAPI (blue) in RCFs under various treatment conditions. Bar plots represent data expressed as mean ± standard error in mean (SEM) along with individual data points from n = 3 independent experiments. Three-way ANOVA followed by multiple comparisons was performed to establish statistical significance. *p<0.05, **p<0.01, ***p<0.001, ****p<0.0001 compared with DMSO control. #p<0.05, ##p<0.01 comparing +TGFβ1 with −TGFβ1 cells within the same treatment group (i.e. 17AAG vs DMSO), &p<0.05, &&p<0.01, &&&p<0.001 comparing cells on 1400 nm patterned topography with cells on planar substrates for same treatment group (±TGFβ).

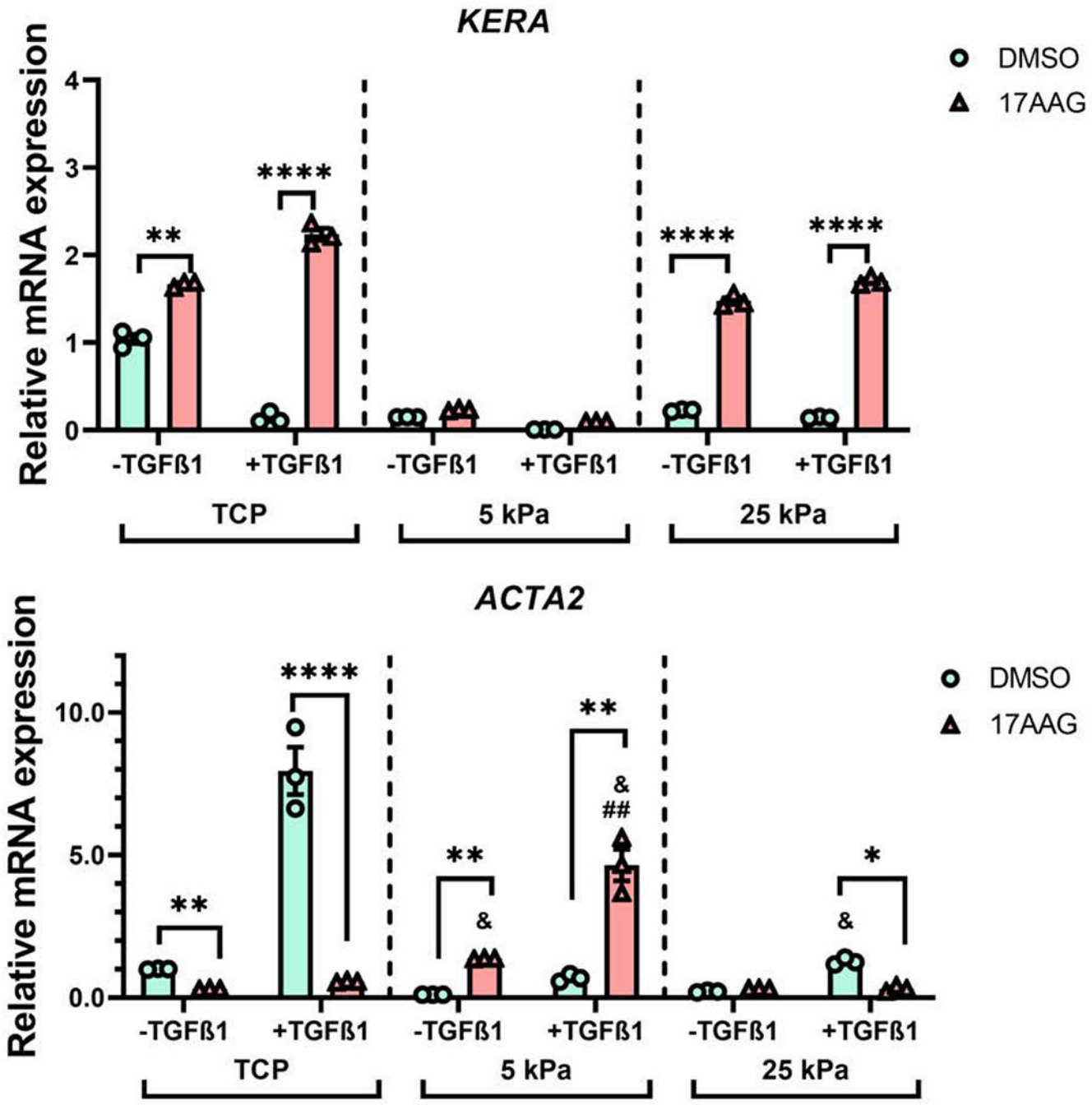


**Figure 7: Substratum stiffness modulates cellular response to Hsp90 inhibition and TGFβ1 treatment.**

Relative mRNA expression in RCFs, cultured on either tissue culture plastic (TCP) or polyacrylamide hydrogels of various elastic moduli (5 kPa *vs.* 25 kPa), treated with DMSO (vehicle control) or 500 nM 17AAG in the presence/absence of 10 ng/ml TGFβ1 for 3 days. Bar plots represent data expressed as mean ± standard error in mean (SEM) along with individual data points from n = 3 independent experiments. Three-way ANOVA followed by multiple comparisons was performed to establish statistical significance. *p<0.05, **p<0.01, ***p<0.001, ****p<0.0001 compared with DMSO control. #p<0.05, ##p<0.01 comparing

+TGFβ1 with −TGFβ1 cells within the same treatment group (i.e. 17AAG vs DMSO), &p<0.05, &&p<0.01, &&&p<0.001 comparing cells on hydrogels with cells on tissue culture plastic substrates for same treatment group (±TGFβ).

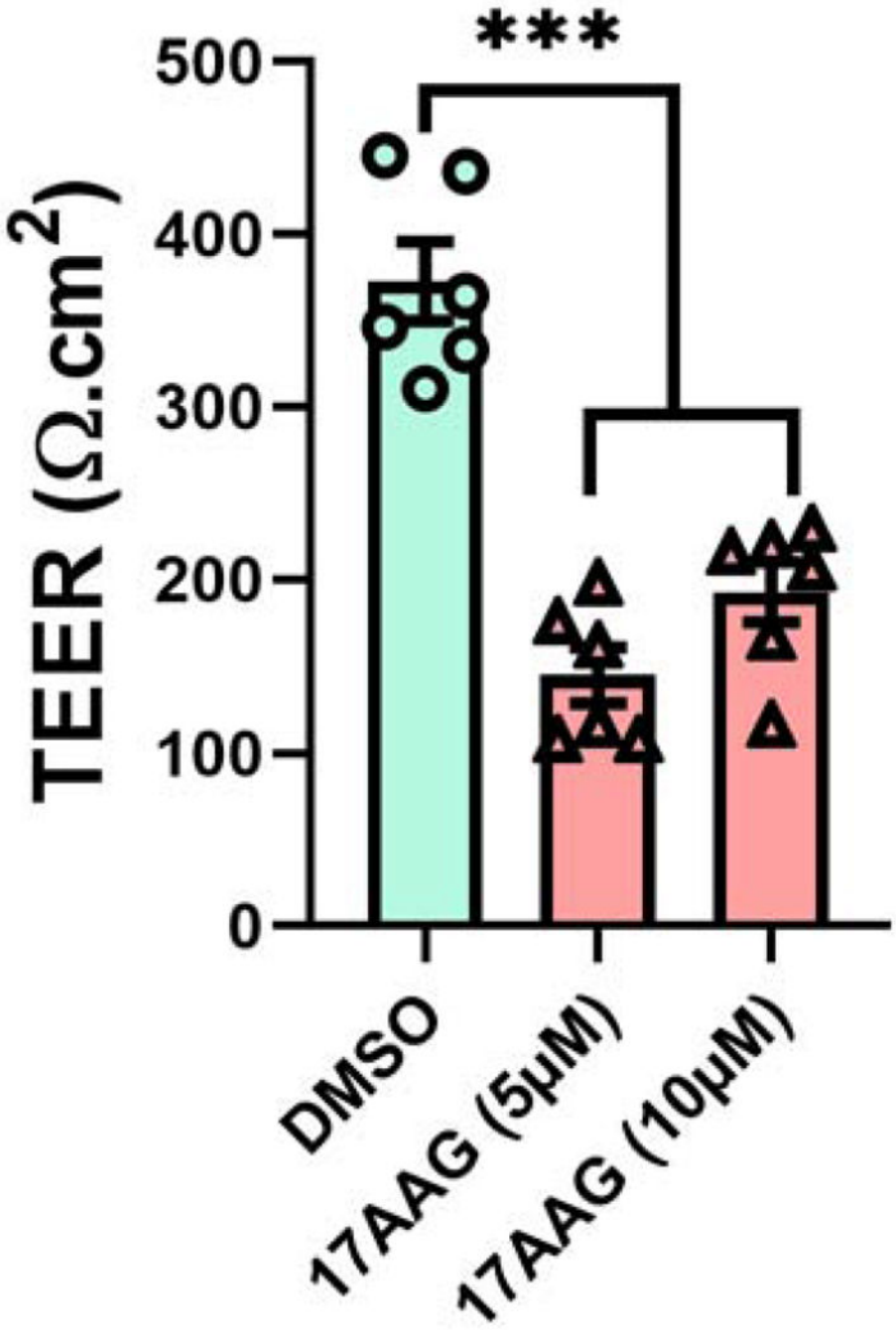


**Figure 8: Hsp90 inhibition disrupts barrier function of stratified corneal epithelial cells.**

Transepithelial electrical resistance (TEER) measured in stratified corneal epithelial cells treated with DMSO (vehicle control) or 17AAG (5 μM, 10 μM) over 24 h. Bar plots represent data expressed as mean ± standard error in mean (SEM) along with individual data points (duplicate) from n = 3 independent experiments. One-way ANOVA followed by Dunnett's multiple comparison test was performed to establish statistical significance. ***$p<0.001$ compared with control group.